XIII Congresso Ibérico de Acústica
55º Congreso Español de Acústica
TECNIACÚSTICA 2024
Faro, 11 a 13 setembro 2024

SIMULATION OF THE ACOUSTIC SCATTERING IN A 2D WAVEGUIDE WITH A DYNAMIC HELMHOLTZ RESONATOR

David Ortega Patón[1], Rubén Picó[2], Jan-Philipp Weiβ[3]

[1] Universidad de Málaga
dort@uma.es
[2] IGIC, Universitat Politècnica de València, Paranfimf, E-46730 Grao de Gandia, Spain
rpico@fis.upv.es
[3] OTH Regensburg
hanphilipp.weiss@oth-regensburg.de

Abstract
Acoustic systems that can change their properties over time establish the base for acoustic space-time metamaterials. Acoustic space-time metamaterials are engineered structures that manipulate sound waves in both space and time and possess unique properties that allow for dynamic control and adaptation of their effective acoustic behavior. By altering the structure or composition of these materials, researchers can influence the propagation, reflection, and absorption of sound waves in intricate ways. This work explores the temporal dynamic behavior of Helmholtz resonators, including time-dependent parameters to tune their acoustics properties. Through the finite element method, the study investigates how the time-dependent variation of the cavity in a Helmholtz resonator affects its acoustic behavior, describing the temporal evolution of this resonator when coupled into a two-dimensional waveguide. According to the first obtained results, this dynamic behavior changes the transmission loss peak position compared to the static case, strongly influenced by the frequency of the cavity variation and its amplitude. This work could help advance the dynamic metamaterials field by investigating their temporal properties and potential in numerous technological fields, holding promise for diverse applications due to their dynamic adaptability.

Key words: dynamic resonators, simulation, transmission loss, time-varying

PACS nº. 43.20.Fn, 43.20.Fn

1 Introduction

A Helmholtz resonator (HR) is an acoustic device comprising a cavity with an open neck, designed to resonate at a specific frequency determined by the cavity volume and neck dimensions, often used to absorb or emit sound at its resonant frequency. The HR is a fundamental model in acoustics and finds extensive application in engineering due to its straightforward design, adaptability, and robustness. Beyond its basic function, the HR's ability to be easily tuned to different frequencies makes it invaluable in various noise control and sound optimization scenarios, enhancing its versatility and effectiveness in practical applications.

The present work aims to provide a study on the transmission phenomena within a two-dimensional acoustic waveguide when a Helmholtz resonator with varying cavity volume is placed between the input and output sides of the waveguide as depicted in Figure 1. This variation of the resonator volume is produced by harmonically moving its backing wall according to a specific frequency, thus changing the HR's resonant frequency over time. This work can serve as a first step into the space-time metamaterials field described in [1] and [2] as the properties of such systems can be varied in space and time to provide new features.

The acoustic damping of a Helmholtz resonator with an oscillating volume was investigated in [3] to be applied as an acoustic damper to stabilize unstable combustion systems. They compare an experimental setup with the numerical results of the waveguide subjected to a low Mach number grazing flow, concluding that the volume oscillation can either increase or decrease the acoustic power absorbed by the resonator depending on the phase that drives the oscillation. In that work, the excitation frequency was fixed at the resonator's resonance, and only phase changes were employed to evaluate the effect in opposition to the present study, where the initial phase is kept constant at 0º, and the varying parameter is the frequency of the moving wall.

The development of this work is entirely based on numerical methods, namely the Finite Element Method implemented with COMSOL Multiphysics®, aiming to explore the acoustic behavior of a time-varying HR. It mainly employs the acoustics module, which plays a major role in current research in acoustics engineering.

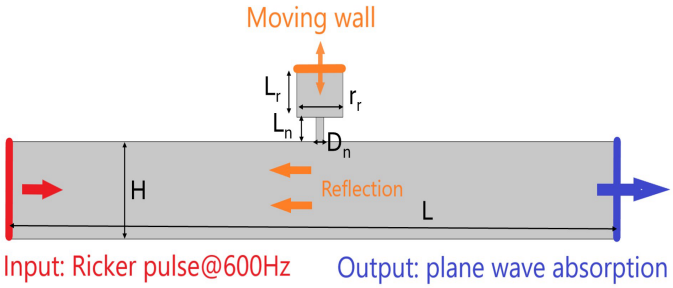

Figure 1: Schematics of the proposed problem

The materials and methods are described in Section 2. The necessary theory to understand this study and the specific boundary conditions applied are defined in Section 3 with more in-depth details regarding the study types in the numerical method. Section 4 offers a discussion and comments based on the results obtained, and Section 5 covers the main takeaways from this work and proposes further steps to continue the research.

2 Materials and methods

This section describes all the steps taken to set up the FEM model to tackle the described problem

2.1 Geometry

The geometry shown in Figure 1 consists of a Helmholtz resonator coupled into an acoustic waveguide. The acoustic waveguide dimensions are set to ensure the propagation of plane waves below 1000 Hz with a diameter H = 0.08 m and a length L = 1 m, as it is the region of interest. The resonator's volume is tuned to resonate at 600Hz (see Section 3) with dimensions of r_r = 3 cm for the radius and L_r = 4 cm as the vertical length (the one that will be varied in time). The diameter of the neck that connects the waveguide to the resonator is set to D_n = 1 cm, and its length L_n = 2 cm. These parameters have been fixed to study the effect of the moving frequency and its amplitude.

2.2 Mesh

The 2D mesh consists of free quad elements, as shown in Figure 2. The final mesh contains 60 quads with an average element quality of 0.98 and a maximum element size of 9 mm. The mesh could be further optimized to reduce the total degrees of freedom as the proposed problem focuses mainly on

low-frequencies; however, it was preferred to leave it like shown in Figure 2 as the total degrees of freedom were less than 2000 in the Time-Domain study with a computational time of less than 4 minutes on average for one frequency (run on an Intel i7-12700H with 32GB of RAM).

2.3 Physics interfaces

The main physics interface used is *Pressure Acoustics, Transient*, which enables the control of the moving wall in the time domain. However, the interface *Pressure Acoustics, Frequency Domain* has also been used to reference and benchmark the static configuration's transmission properties (with no movement at the resonator's upper wall).

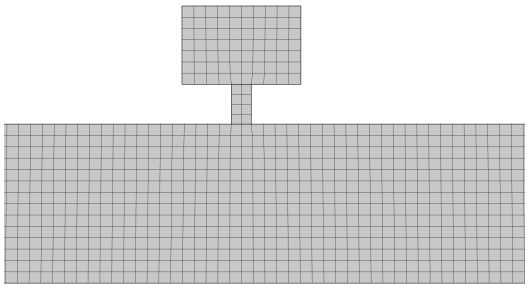

Figure 2: Mesh for the proposed problem.

The input and output boundary conditions are set with the *Plane Wave Radiation* boundary feature, giving the input boundary the property of *Incident Pressure Field* with a *User defined* pressure field type that enables the control of the input energy to the system. This pressure field is created as a Ricker wavelet pulse defined in Section 3 and implemented via an analytic function with a center frequency at the resonator's resonance frequency. Applying this boundary condition makes absorption possible at both ends of the waveguide, thus avoiding reflections. The rest of the boundaries are set to *Sound Hard Boundary (Wall)*. The material applied to the domain is air with c= 343m/s and ρ =1 .21kg/m^3. This work does not consider dissipation due to thermo-viscous losses in the narrow region as it would have to be manually implemented in the *Pressure Acoustics, Transient* interface via a complex sound speed and is not a goal for this preliminary study.

2.4 Moving mesh

To model the cavity's moving wall, the *Moving Mesh* interface is needed to account for the domain's dimension change at each time instance. A prescribed deformation in the vertical direction y is applied at the boundary with a sinusoidal harmonic movement $f(t) = A_{mov}\sin(2\pi \cdot f_{mov}t)$, with amplitude A_{mov}, and frequency f_{mov}. Moreover, a *Deforming Domain* is applied to the resonator's cavity 2D domain with a *Yeoh* mesh smoothing type with a stiffening factor of 10 and no initial deformation as shown in Figure 3.

The moving mesh is shown in Figure 4 at two different time instances to evaluate the mesh under compression or a stretch. Both are considered to have good quality for the present study, although further refinement of the corners (especially for the compression case) is advised as the next step. To observe the effect on the transmission with different moving frequencies of the wall, the movement of this boundary will be of 1 cm of amplitude at 10Hz, 30Hz, 60Hz, 300Hz, 600Hz, and 720Hz. However, it is preferred to reference the moving frequency f_{mov} to the resonant frequency of the excitation f_{res} as $\beta = \frac{f_{mov}}{f_{res}}$, resulting in ratios of β = 0.016, 0.05, 0.1, 0.5, 1, and 1.2.

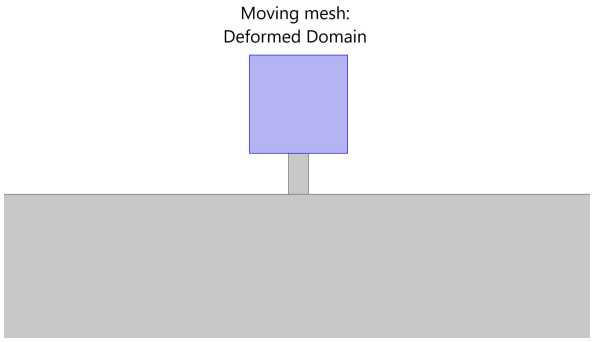

Figure 3: Deformed domain within the moving mesh property.

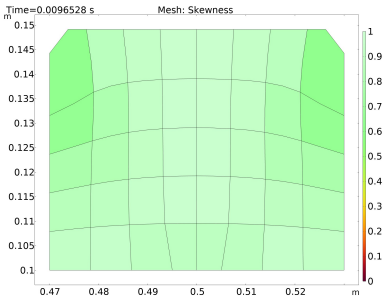

(a) Stretched mesh.

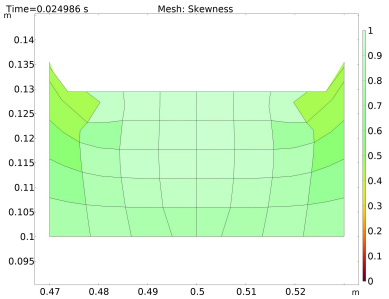

(b) Compressed mesh

Figure 4: Skewness of the moving mesh at two different time instants.

Moreover, a separate case where the moving frequency is fixed to β = 0.016 (10 Hz) is carried out with varying amplitude of the movement, defined by the relative term $\alpha = \frac{A_{mov}}{L_r}$ with values of α = 0.025, 0.25, 0.5, and 0.76, corresponding to absolute amplitudes of 1 mm, 1cm, 2 cm, and 3 cm respectively.

3 Theoretical background

The theoretical foundation of the problem is described in this section, covering the underlying partial differential equations used by the Finite Element Method and the most relevant theoretical concepts describing the Helmholtz resonator.

3.1 Numerical studies

The dependent variable solved for in all the used studies is the acoustic pressure. However, the equations that define this pressure are different for the frequency and time domain studies, thus they are reviewed in the following sections.

3.1.1 Frequency dependent

This study employs the inhomogeneous Helmholtz equation solved for the pressure $p(\mathbf{x}) = p(x,y)e^{-ikz}$:

$$\nabla \cdot (-\frac{1}{\rho}(\nabla p_t - \mathbf{q}_d)) - \frac{k_{eq}^2 p_t}{\rho} = Q_m \tag{1}$$

where ρ is the density of the medium (non-complex value for the present case), $p_t = p + p_b$ is the total pressure with p_b being the background pressure, k_{eq} is the wave number defined as $k_{eq}^2 = \left(\frac{\omega}{c}\right)^2 - k_z^2$, with k_z being the out-of-plane wave number set to 0, c is the sound speed (non-complex in this case), and $\boldsymbol{q}_d$ and Q_m are dipole and monopole sources, respectively.

The first study was done in the frequency domain due to its simplicity and computational efficiency to serve as a reference and benchmark for the subsequent time domain simulation. Thus, no movement of the resonator's wall was implemented due to the static nature of the analysis. The input and output are modeled through the *Port* boundary condition of the *Slit* type that model the plane wave mode, being the input enabled for incident wave excitation. This boundary condition establishes the total acoustic pressure p_t at a given boundary following the expression:

$$p_t = \sum_{i \in bnd} A^{in} e^{i\Phi}\left(S_{ij} + \delta_{ij}\right)p_i \tag{2}$$

where the summation i is over all ports on the given boundary bnd, S_{ij} is the components of the scattering matrix, p_i is the port mode shape of the i-th port, A^{in} is the amplitude, ϕ is the phase of the incident wave (source). The rest of the boundaries are defined by a null transverse velocity.

3.1.2 Time dependent

The transient study consists of only one step: *Time Dependent*. A *Direct* time-dependent solver is chosen using a *Generalized alpha* method with a free time stepping strategy. It provides higher accuracy with less damping than order methods such as BDF (see [4] for more information regarding time-dependent studies). This time step is applied to both physics interfaces (Pressure Acoustics and Moving mesh) via a *Fully Coupled* direct linear solver with an Automatic Newton nonlinear method.

The Time-Dependent study models a transient phenomenon in a stationary fluid by solving the following equation for the acoustics pressure $p = p(x,t)$

$$\frac{1}{\rho c^2}\frac{\partial^2 p}{\partial t^2} + \nabla \cdot (-\frac{1}{\rho}(\nabla p - \mathbf{q}_d)) = Q_m \tag{3}$$

The *Plane Wave Radiation* boundary condition is used for both the input and output having the former the extra node of *Incident Pressure Field* which creates the incident pressure p_i as a plane wave following $p_i = p_0 \cdot e^{-\mathrm{kx}}$, where p_0 is the wave amplitude, k is the wave vector, and x is the location on the boundary. The waveguide excitation is done by a single pulse with a Ricker wavelet shape. The Ricker wavelet pulse pressure field $f(t)$ as a function of time t is defined as

$$f(t) = (1 - 2\pi^2 f_M^2 (t - t_0)^2)e^{-\pi^2 f_M^2 (t-t_0)^2} \tag{4}$$

where f_M is the center frequency of the pulse, and t_0 is the time delay of the pulse. The time domain pressure amplitude of such pulse is shown in Figure 5a with its FFT in Figure 5b.

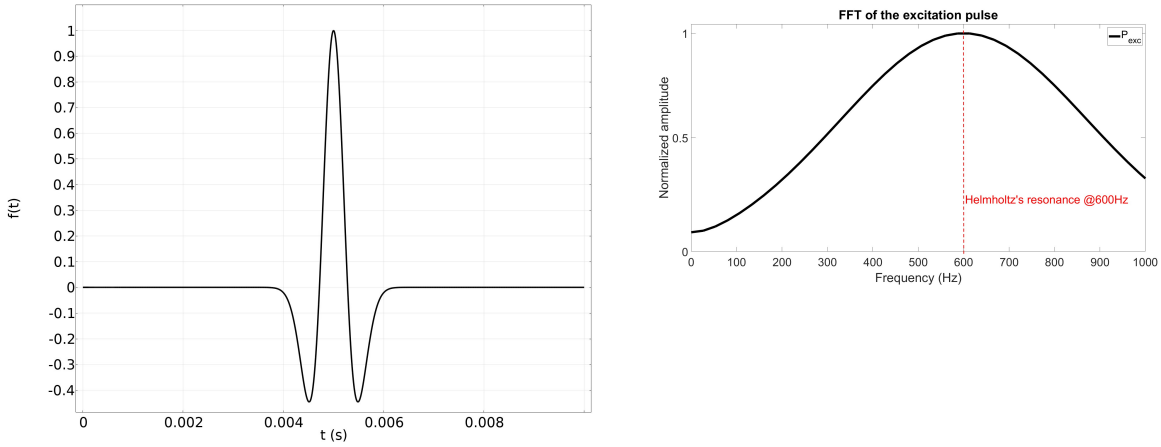

Figure 5: Time and frequency domain plots of the excitation signal. a) Time domain plot of the Ricker pulse with a center frequency fM =600 Hz. b) FFT of the excitation pulse.

In order to evaluate the system's behavior at different frequencies of the moving wall, a *Parametric Sweep* is added to the study.

3.2 Helmholtz resonators

As summarized in [5], an HR consists of a narrow neck connected to an air volume cavity as shown in 6. The mass of air in the neck $M_m = \rho_0 S_n L_{eq}$ is thus connected to the cavity that acts as a massless spring with stiffness $K_n = \rho_0 c_0^2 S_n^2 / V_c$ driven by an external sound pressure force $F = S_n p_0 \cdot e^{j\omega t}$, where p_0 is the oscillation sound pressure, ρ_0 and c_0 the air density and sound speed, respectively, L_{eq} and S_n are the neck's effective length and cross-sectional area respectively, ω is the angular frequency, and V_c is the cavity volume. From this, the resonant frequency f_{res} of a Helmholtz resonator is given by [6]

$$f_{res} = \frac{c}{2\pi}\sqrt{\frac{S_n}{V_c L_{eq}}}, \tag{5}$$

where $L_{eq} = L_n + 0.7 D_n$ is the equivalent (corrected) length of the neck, with L_n being the actual length of the neck and D_n the neck diameter. Due to the twodimensional nature of the problem being solved, the volume V_0 is changed to the surface of the resonator S_{res}, and the cross-sectional area of the neck S_n is changed to the diameter of the opening D_n, thus resulting in

$$f = \frac{c}{2\pi}\sqrt{\frac{D_n}{S_{res} L_{eq}}} \tag{6}$$

Due to inaccuracies in this 2D translation of the problem, the correction factor applied to the length with the value of 0.7 is adjusted to be 5 to match the expected resonance to the one resulting from the simulation. This was carried out by adjusting this correction factor until it matched the desired value.

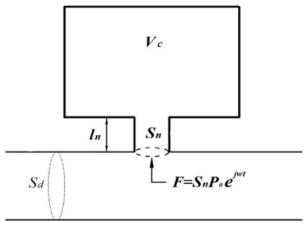

Figure 6: Schematics of the HR (taken from [5]).

3.3 Transmission and reflection coefficients

The analysis will be based on the transmission and reflection coefficients and the transmission loss to evaluate the performance of the Helmholtz resonator placed in the waveguide. The transmission coefficient *T* is calculated as

$$T = \frac{|P_{out}|^2}{|P_{exc}|^2}, \tag{7}$$

where P_{out} is the fast Fourier transform (FFT) of the pressure at the output boundary, and P_{exc} is the FFT of the excitation signal at the input, the Ricker pulse. The excitation pressure is extracted from COMSOL® as the variable *actd.p_i* corresponding to the pressure of the *Plane Wave Radiation* feature. The input and output boundary pressures are extracted using the average operator for the *actd.p* variable in the time domain case, and the variables *acpr.port1.P_in* and *acpr.port2.P_out* for the input and output, respectively, for the frequency domain case. The reflection coefficient *R* is calculated as

$$R = \frac{|P_{reflected}|^2}{|P_{exc}|^2}, \tag{8}$$

where $P_{reflected}$ is the FFT of the reflected pressure from the resonator at the input boundary. $P_{reflected}$ is calculated as the total received pressure over all the computed time at the input boundary minus the pressure generated with the excitation's Ricker pulse.

As the analysis covers a dynamic system due to the moving wall of the resonator, there is some energy that gets introduced into the system or dissipated by interference phenomena. To account for this energy, a coefficient of external energy *D* can be defined as

$$D = T + R - 1, \tag{9}$$

where a positive value of *D* would mean that energy is introduced externally to the system by the dynamic resonator, and a negative value would mean dissipating that energy. Finally, the transmission loss *TL* in dB is calculated as

$$TL = 20 \cdot log(\frac{|P_{exc}|^2}{|P_{out}|^2}) \tag{10}$$

4 Results and discussion

Most of the calculated pressure field postprocessing has been carried out with Matlab through the *LiveLink* interface provided by the COMSOL® 's license. The postprocessing consists of a basic signal processing chain shown in the schematics of Figure 7. The presented results follow the described case studies proposed in Section 2.4. The band-pass filtering focuses the analysis only in the desired frequency range where the excitation signal has the main energy. Moreover, an offset due to a low-frequency component was observed during the postprocessing and solved with low-pass filtering.

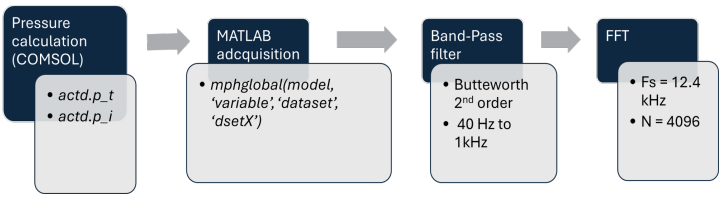

Figure 7: Schematics of the postprocessing done with MATLAB LiveLink

4.1 Static configuration: Frequency domain and time-dependent studies

The benchmark test that serves as a reference for the time-dependent subsequent studies is shown in Figure 8. The agreement between both studies is observed, thus confirming the accuracy of the Time Domain study after computing the postprocessing chain.

As a first example, Figure 9a shows the time domain plots of the excitation signal, the reflected pressure, and the pressure at the output when there is no movement (static case). The reflection created by the Helmholtz resonator can be clearly observed in this figure. The FFT of the previous signals is shown in Figure 9b, showing how the reflection frequency content is at the resonant frequency of the Helmholtz resonator as expected. At the same time, the output lacks exactly this frequency content. The transmission loss of this static case is shown in Figure 10 with a narrow peak at the resonant frequency and will, from now on, serve as a reference to assess the performance of the dynamic case compared to the static one.

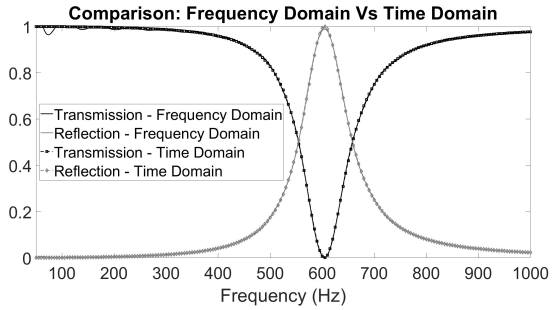

Figure 8: Time Domain and Frequency Domain studies comparison.

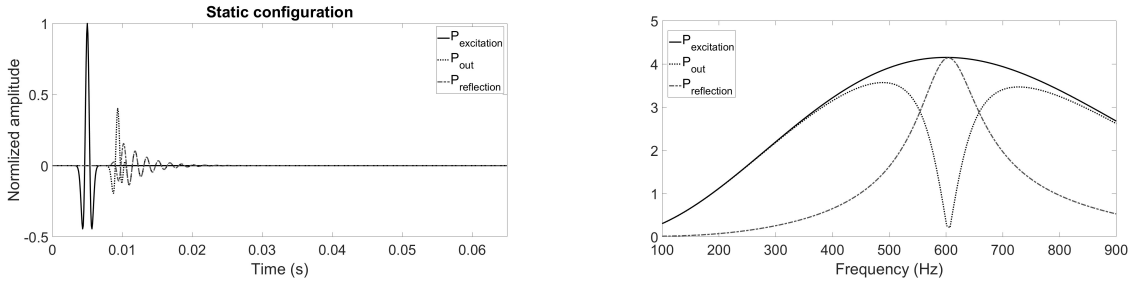

Figure 9: Time and frequency domain plots of the static signals. a) Time domain waves of the static case and b) FFT of the static case signals.

The 2D FFT can be computed thanks to the study step *Time to Frequency FFT*. This way, it is possible to check, spatially, how this resonance happens, as shown in Figure 11 for the resonant frequency of 600Hz. It shows how this frequency is effectively not transmitted and reflected by the resonator, thus producing the aforementioned transmission loss peak.

4.2 Dynamic configuration

The results implying the moving wall are discussed in this section. As a general example of the time domain behavior, Figure 12 shows the reflected signal at $\beta = 0.1$ compared to the static case, observing the change in amplitude and frequency that will affect the transmission. This effect is observed in all the tested frequencies.

To see how the pulse travels within the geometry and the deformed domain of the resonator, Figure 16 shows the 2D geometry at various time snaps, capturing the main idea of the study.

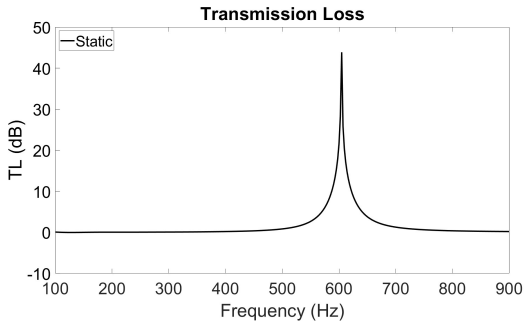

Figure 10: Transmission loss for the static case.

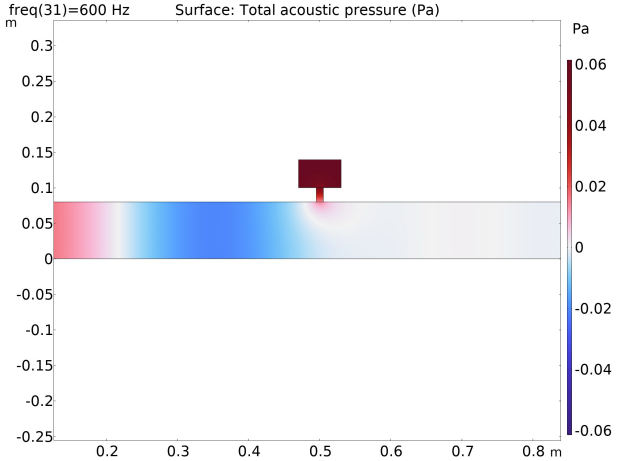

Figure 11: 2D FFT at the resonant frequency (600Hz) for the static case.

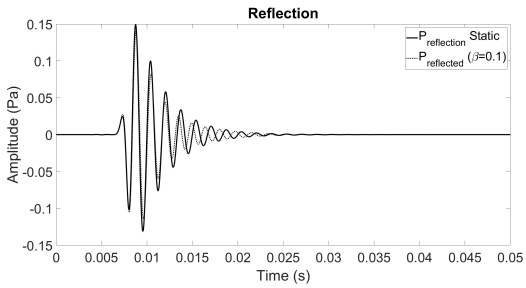

Figure 12: Time domain reflection waves for the static and $\beta = 0.1$ cases.

4.2.1 Low frequency regime (β ≤ 0.1)

The first part of the analysis is based on the low-frequency regime where the frequency of the moving wall only goes up to 10% of the resonator's resonance ($\beta \leq 0.1$). The displacement of 1 cm at the resonator's wall produces a change in the total surface, thus having two new resonant frequencies at the maximum absolute value of the displacement: f_{min} at 540 Hz, and f_{max} at 700Hz. These three frequencies will always be marked to serve as a reference. The reflection coefficient for $\beta \leq 0.1$ is shown in Figure 13. It is observed a shift on the reflection peak within the region $f_{min} < f < f_{max}$ compared to the static case.

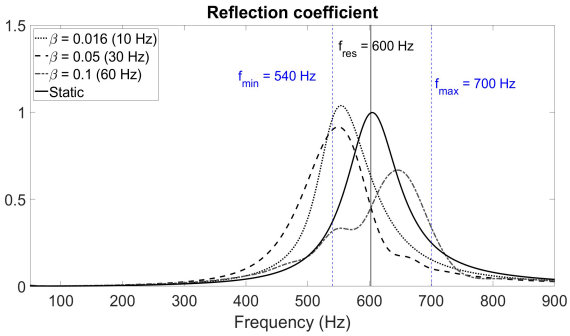

Figure 13: Reflection coefficient in the low-frequency regime with vertical lines showing the HR's resonant frequency f and the two extreme frequencies f_{min} and f_{max} corresponding to the new resonance produced by the decrease or increase of the HR's volume respectively.

Regarding the transmission loss, shown in Figure 14, the peaks appear to have the same tendency as the reflection coefficients. However, it is observed that for the case $\beta = 0.1$, the peak maximum value is drastically reduced, but its bandwidth increased. A closer look into this plot reveals negative transmission loss values, meaning an enhancement at certain frequencies. This can be caused by the introduction of the movement at the resonator's wall, as the system is no longer conservative.

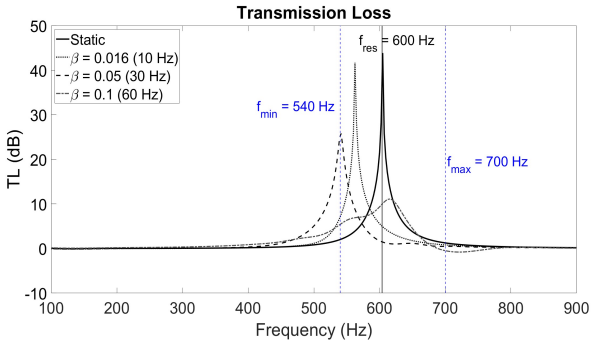

Figure 14: Transmission Loss in the low-frequency regime.

In an attempt to understand this behavior better, the external energy coefficient D is shown in Figure 15. It is worth mentioning that for the case where $\beta = 0.1$, the positive values of D match with the amplification shown in the transmission loss, where the dissipation (negative values of D) corresponds with the positive values of the transmission loss, where energy is effectively not transmitted. A similar convention seems to be happening for the lower β cases, although confirming this would require a more in-depth analysis of such a case.

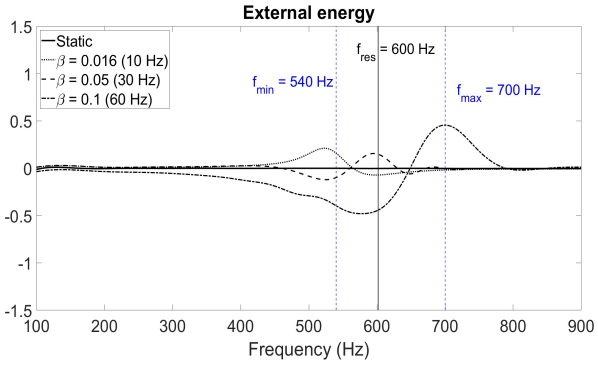

Figure 15: External energy in the low-frequency regime.

4.2.2 Low frequency regime (β=0.016) and α ≤ 0.75

A second case is offered where β remains constant and this time is the relative amplitude α the varying parameter. Figure 17 shows the transmission loss results for 4 different values of α compared to the static case. The main conclusion that can be drawn here is that the amplitude of the wall's movement considerably affects the output. However, none of the new transmission loss peaks appear to be higher in frequency than the central absorption peak provided by the static case, and they all fall within the range $f < f_{res}$. The interpretation of these results suggests that the transmission phenomena are ruled by the moment (or the time range) at which the Ricker pulse arrives at the HR, being the peak of absorption linked to the volume (surface in this case) of the resonator at that time instant. This can be analyzed by considering that the distance between the input and the HR is 0.495 m, thus needing 1.4 ms for the pulse to arrive at the HR. At this instant, the amplitudes of the moving wall have the values shown in Figure 18. Being the amplitude of the movement at that time instant of 6.6 mm for the $\beta = 0.1$ case, the length of the resonator will be increased by 5 mm, thus resulting in a resonant frequency of 555 Hz. However, this still doesn't explain the position of other peaks as they might be influenced by other physical effects, and thus, analyzing this behavior is part of the further steps defined in the next section.

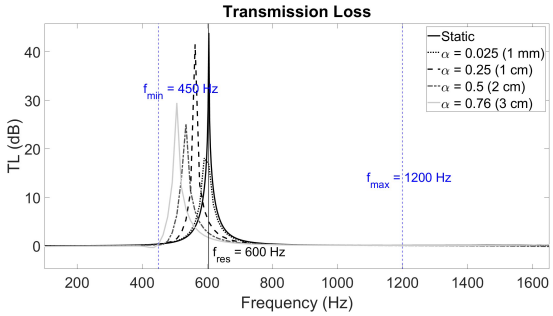

Figure 17: Transmission loss for a constant moving frequency of $\beta = 0.016$ (10 Hz) and different values of α

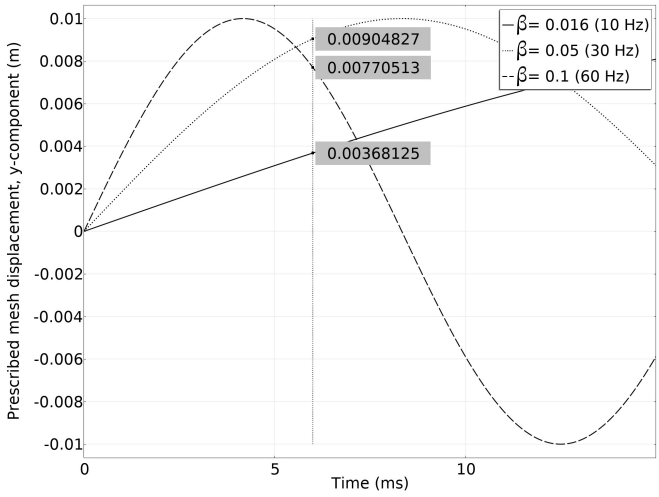

Figure 18: Displacement of the moving wall at the low-frequency regime $\beta \leq 0.1$.

5 Conclusions

This work has developed a preliminary study on the effect of a varying volume Helmholtz resonator in the transmission when coupled to a waveguide. The study was performed at frequencies below the HR resonance (up to 10% of the resonance frequency). For this case, a displacement of the transmission loss peak has been observed, which could be ruled by the position of the moving wall when the pulse meets the resonator as a potential hypothesis. The results of this study suggest that a dynamic resonator has the potential to control the transmission without adding any extra elements, although the main physics principle used to describe this phenomenon is not yet well understood. Moreover, the presented development highlights the importance of the external energy added to the system (and making it no longer conservative) as a potential candidate to accurately describe the system's behavior.

The presented results in this work just establish the first steps towards a full analysis to understand this dynamic system's behavior in spacetime metamaterials. Thus, as a continuation in the field, these are the proposed next steps:

- Increase the system's complexity by including multiple resonators in series, with independent control of their moving walls in a finite system or analyze the dispersion relation of a periodic system using the dynamic resonator as a unit cell.
- Assess the influence of more parameters, such as the amplitude of the moving wall or the resonator's neck dimensions.
- Employ different types of excitation signals like pulse trains.

- Include the thermo-viscous losses produced in the neck of the resonator by introducing a complex sound speed.
- Account for the acoustic pressure generated by the moving wall.

Acknoledgments

This work was supported by the Spanish Ministry of Science and Innovation (MICINN) and the European Union FEDER (project PID2022-138321NB-C22).

References

[1] C. Caloz and Z.-L. Deck-Leger, "Spacetime metamaterials—part i: General concepts," *IEEE Transactions on Antennas and Propagation*, vol. 68, no. 3, pp. 1569–1582, mar 2020. [Online]. Available: https://doi.org/10.1109%2Ftap.2019.2944225

[2] C. Caloz and Z.-L. Deck-Léger, "Spacetime metamaterials—part ii: Theory and applications," *IEEE Transactions on Antennas and Propagation*, vol. 68, no. 3, pp. 1583–1598, 2020.

[3] D. Zhao, C. A'barrow, A. S. Morgans, and J. Carrotte, "Acoustic damping of a helmholtz resonator with an oscillating volume," *AIAA Journal*, vol. 47, no. 7, pp. 1672–1679, 2009. [Online]. Available: https://doi.org/10.2514/1.39704

[4] "Comsol multiphysics reference manual 6.2," pp. 1442–1765, 2023. [Online]. Available: https://doc.comsol.com/6.2/doc/com.comsol.help.comsol/COMSOL_ReferenceManual.pdf

[5] C. CAI and C. M. MAK, "Noise attenuation capacity of a helmholtz resonator," *Advances in Engineering Software*, vol. 116, pp. 60–66, 2018. [Online]. Available: https://www.sciencedirect.com/ science/article/pii/S0965997817310293

[6] L. Kinsler, A. Frey, A. Coppens, and J. Sanders, *Fundamentals of Acoustics*. Wiley, 2000. [Online]. Available: https://books.google.at/books?id= FecSEAAAQBAJ